Journal of Research and Applications in Mechanical Engineering
ISSN: 2229-2152 (Print); 2697-424x (Online)
(2026) Vol. 14, No. 1, Paper No. JRAME 26-14-003
[DOI: 10.14456/ jrame.2026.3]

Research Article

Enhancement of Vickers hardness and Electrical Conductivity in 3YSZ-8YSZ Oxide System with Al_2O_3 Addition

X. Rong [1]
S. Zhu [2]
K. Takeshi [2]
M. Yoshinaga [3, *]
[1] *Department of Mechanical Engineering, Graduate School of Engineering, Tokai University, Kanagawa, 259-1207, Japan*
[2] *Department of Prime Mover Engineering, Tokai University, Kanagawa, 259-1207, Japan*
[3] *Department of Mechanical Systems Engineering, Tokai University, Kanagawa, 259-1207, Japan*

Received 14 August 2024
Revised 23 January 2025
Accepted 1 February 2025

Abstract:
Solid oxide fuel cells (SOFC), primarily composed of oxide materials, operate at temperatures ranging from 600 to 1000°C. Yttria-stabilized zirconia (YSZ) has high oxide ion conductivity at 900°C, making it a promising material for SOFC electrolytes and anode electrodes. In this study, Al_2O_3 was added to 3YSZ-8YSZ oxides, and the electrical conductivity and Vickers hardness were evaluated. Recommended values for the amounts of 3YSZ, 8YSZ, Al_2O_3, and sintering temperature were obtained by machine learning. The recommended value determined from the electrical conductivity, Vickers hardness, and sintering temperature of C0(50.0wt% 3Y-50.0wt% 8Y-0wt% Al_2O_3), C05(49.7wt% 3Y-49.7wt% 8Y-0.50wt% Al_2O_3), and C1(49.5wt% 3Y-49.5wt% 8Y-1.0wt% Al_2O_3), and other related samples. The recommended composition was determined to be R1 (48.8wt% 3Y-50.8wt% 8Y-0.35wt% Al_2O_3), and the sintering temperature was 1410°C. The crystal structure of R1 was cubic structure indexed as ICDD PDF # 00-030-1468. The electrical conductivity of R1 was observed to be more than 1000 times higher than that of sample C0 without alumina added.

Keywords: *SOFC, YSZ, Composite material, Electrolyte.*

1. Introduction

Fuel cells are attracting attention as a new energy system to replace traditional fossil fuel energy systems. Solid oxide fuel cells (SOFC) are made of ceramics and have a high operating temperature of 600 to 1000°C. SOFCs are anticipated to be used in highly energy-efficient and environmentally friendly cogeneration systems. They convert the chemical energy of the fuel directly into electrical energy, achieving high energy conversion efficiency. SOFCs can utilize various fuels; while hydrogen and hydrocarbons are commonly used, other fuels such as natural gas and biogas can also be employed, thus broadening the range of fuel options.

The electrolyte must allow the movement of oxide ions (O^{2-}) between the electrodes. Additionally, to avoid short-circuiting of the cell, the electrolyte must have low electronic conductivity. Therefore, the basic requirements for electrolyte materials include high oxide-ion conductivity, low electronic conductivity, sinter ability, chemical stability, and mechanical strength. The most used material to meet these requirements is stabilized zirconia. Doping zirconia (ZrO_2) with larger cations and cubic system oxides (such as CeO_2 and Y_2O_3) helps to suppress phase transitions, allowing the high-temperature phase structure to be maintained at lower temperatures. Zirconia has a very high melting point and undergoes structural phase transitions. Below 1440 K, it has a monoclinic fluorite-type structure ($P2_1/c$, Z=4).

* Corresponding author: M. Yoshinaga
E-mail address: yoshinaga@tokai.ac.jp

Between 1440 K and 2640 K, it adopts a tetragonal fluorite-type structure ($P4_2/nmc$, Z=2), and from 2640 K to its melting point (2940 K), it possesses a cubic fluorite-type structure (Fm3m, Z=4). The crystal structure of YSZ is the fluorite-type structure [1].

The regression model was performed using the experimentally measured oxide-ion conductivity and Vickers hardness for the ternary composition, 3YSZ-8YSZ-Al_2O_3, as the training data set. The model was trained to predict the sintering temperature and oxide-ion conductivity from ternary composition. Here, we used Gaussian process regression as implemented in the COMBO (Common Bayesian Optimization library) package, which is an open-source Python library designed to implement efficient Bayesian optimization. It employs techniques such as Thompson sampling, random feature maps, one-rank Cholesky update, and automatic hyperparameter tuning, aimed at accelerating scientific discovery, particularly in fields like chemistry and physics. COMBO can handle large-scale training data and has been applied to problems such as determining the atomic structure of a crystalline interface, demonstrating its effectiveness. [2] Gaussian processes can estimate uncertainties in addition to predictions. In the COMBO package, random feature maps are used, which approximate a random mapping. To achieve fast computation, a random feature map is used that approximates the mapping induced by the Gaussian kernel. [3] The hyper-parameters are automatically determined by maximizing the Type-II likelihood.

YSZ is a material composed of a mixture of Y_2O_3 (yttria) and ZrO_2 (zirconia). 8YSZ refers to a composition of 8 mol% Y_2O_3 and 92 mol% ZrO_2, while 3YSZ refers to 3 mol% Y_2O_3 and 97 mol% ZrO_2. 3YSZ is commonly used to adjust composite materials with other engineering ceramics such as Al_2O_3. In contrast, 8YSZ exhibits the best ionic conductivity and excellent chemical stability over a wide temperature and oxygen partial pressure range. Samples containing 20wt%, 25wt%, and 35wt% 3YSZ were tested for flexural strength and fracture toughness. The results showed that the addition of 3YSZ inhibited the growth of cubic phase grains, resulting in smaller cubic phase grain sizes in the composite samples compared to the pure 8YSZ samples. Research indicates that adding 3YSZ particles to an 8YSZ matrix reduces the matrix conductivity at high temperatures ($T > 550$ °C), whereas conductivity improves at lower temperatures ($T < 550$ °C). The electrical conductivity of the composite specimens increased as the 3YSZ content rose from 0wt% to 50wt%. However, when the 3YSZ content exceeded 50wt%, the electrical conductivity decreased. It was found that a 1:1 mass ratio of 3YSZ to 8YSZ can achieve both Vickers hardness and electrical conductivity. [4]

In experiments adding a small amount of Al_2O_3 to 3YSZ, when the Al_2O_3 content is low (e.g., <2 wt%), Al^{3+} ions segregate at the zirconia grain boundaries, facilitating the implementation of the volume diffusion mechanism and thus improving the densification process of the ceramic. Enhanced densification improves Vickers hardness. However, when the Al_2O_3 content exceeds the solubility limit (0.1–0.3wt%), excessive Al_2O_3 accumulates at the zirconia grain boundaries, hindering the diffusion of Zr^{4+} ions and causing the diffusion mechanism to shift to grain boundary diffusion, which reduces sintering efficiency. Appropriate addition of Al_2O_3 was able to enhance the mechanical properties of ceramics, but excess Al_2O_3 negatively affected the diffusion process, impacting the final material properties. [5]

The conductivity decreased when the Al_2O_3 content increased from 0 to 20wt%. [6] However, there are few detailed analyses of solid solution of alumina in YSZ below 0.5wt%. In this study, we attempted to add alumina to 3YSZ-8YSZ oxides. The best estimates of the amount of alumina and the sintering temperature of the disks were calculated by machine learning.

2. Experimental

The experimental time was significantly shortened through automatic improvement by using the Gaussian process regression model on a computer, which was reported by Tsuyoshi Ueno et al. [2][3] This model aims to search for the optimal mixture components, ratios, and process conditions for multiple required properties from a vast number of combinations. When we are adding Al_2O_3 to the YSZ system, there are 50,015,001 possible combinations even when exploring in increments of 0.01%. The proposed method is demonstrated in Fig. 1, where the horizontal axis represents hardness and electrical conductivity, and the vertical axis represents frequency. The four blue circles represent experimental values. This value must be measured in advance. The maximum value was estimated by calculating 5000 Gaussian regression curves for standard deviations of arbitrary width. In Figure 2, the blue circles indicate recommended values, and the white circles indicate measurement points. It is possible to generate new data points that deviate from the original data by increasing the standard deviation. The process plane was fixed at the

determined recommended process conditions, and multiple points on the same process plane were sampled to improve the accuracy of the machine-learning model. This approach significantly reduced the experimental time.

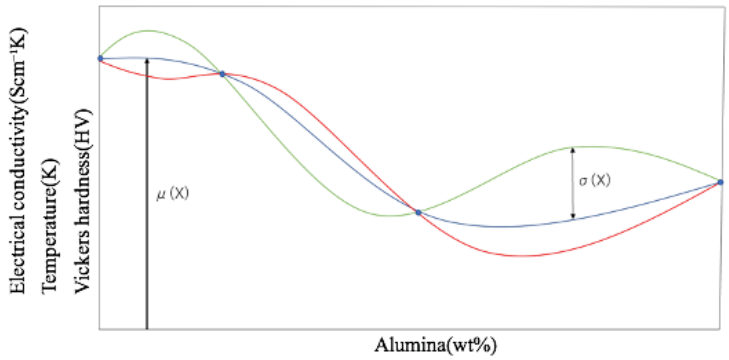

Fig. 1. Gaussian process regression model.

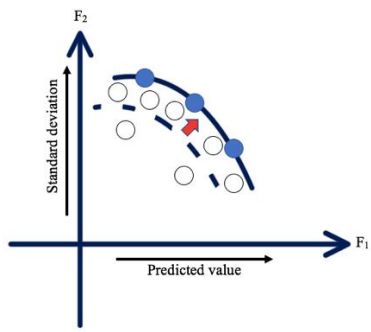

Fig. 2. Exploration techniques

0, 0.5, 1.0wt% of Al_2O_3 was added to the 3YSZ-8YSZ oxide system with a mass ratio of 1:1, respectively, and then the Vickers hardness and electrical conductivity were determined by experiment and used as initial data for calculations. The conductivities and Vickers hardness for the composition ratios of the initial samples are shown in Table 1. In addition, the electrical and mechanical properties of samples with various 3YSZ/8YSZ ratios without any Al_2O_3 addition were evaluated to enrich the dataset and improve the robustness of the optimization process. Samples *A1(0wt% 3Y-100wt% 8Y), A2(10wt% 3Y-90wt% 8Y), A3(25wt% 3Y-75wt% 8Y), A4(35wt% 3Y-65wt% 8Y), A5(50wt% 3Y-50wt% 8Y), A6(65wt% 3Y-35wt% 8Y), A7(75wt% 3Y-25wt% 8Y), A8(90wt% 3Y-100wt% 8Y), A9(100wt% 3Y-0wt% 8Y) were sintered at 1400 °C, whereas A10(0wt% 3Y-100wt% 8Y), A11(10wt% 3Y-90wt% 8Y), A12(25wt% 3Y-75wt% 8Y), A13(35wt% 3Y-65wt% 8Y), A14(100wt% 3Y-0wt% 8Y) were sintered at 1350 °C.* Starting with known samples, we utilized Hiplot and performed Bayesian Optimization (BO). During the optimization process, we excluded options with Vickers hardness below 1187 HV to ensure the material possesses the fundamental mechanical strength required as an electrolyte for SOFC. In our BO, a total of 10 samples were recommended, with their composition ratios and fabrication temperatures displayed in Table 2. Ultimately, we selected sample No.4 with the highest electrical conductivity as our target material (recommended value), as shown in Fig. 3.

Table 1: Initial samples whose composition ratios (3YSZ, 8YSZ, Al_2O_3) in percentage and their conductivities and Vickers hardness were measured at 900 °C.

Sample No.	**Ratio (3YSZ, 8YSZ, Al_2O_3) wt%**	**Conductivity S cm^{-1} K**	**Vickers hardness HV**
1	(50, 50, 0)	2.6	1420
2	(49.7, 49.7, 0.5)	4.1	1243
3	(49.5, 49.5, 1.0)	2.9	1213

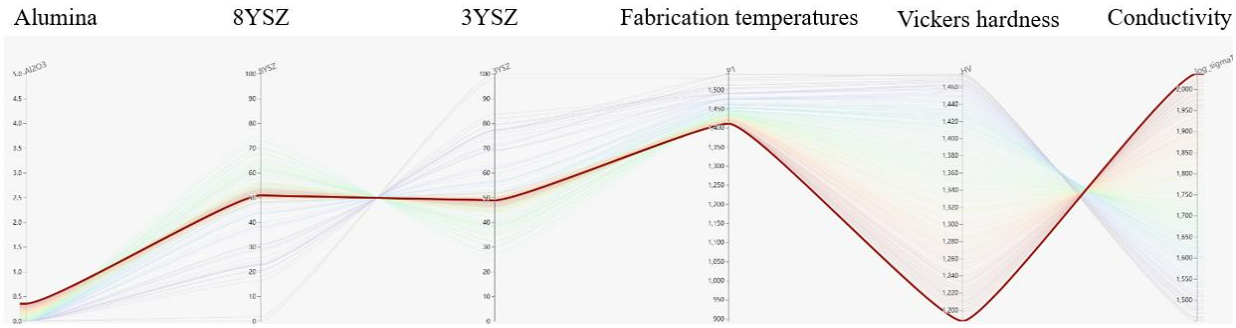

Fig. 3. Result of Bayesian optimization

Table 2: Recommended samples by BO, whose composition ratios (3YSZ, 8YSZ, Al_2O_3) in percentage and their conductivity, Vickers hardness, and fabrication temperatures.

Sample No.	Ratio (3YSZ, 8YSZ, Al_2O_3) wt%	Conductivity S cm^{-1} K	Temperature K	Vickers hardness HV
4	(48.8, 50.8, 0.35)	2.036	1410	1187
5	(46.6, 53.2, 0.18)	1.829	1425	1299
6	(46.5, 53.2, 0.24)	1.918	1417	1254
7	(44.5, 55.3, 0.12)	1.753	1429	1339
8	(38.4, 61.4, 0.12)	1.759	1433	1335
9	(48.4, 51.4, 0.15)	1.788	1422	1318
10	(68.9, 31.1, 0)	1.509	1489	1458
11	(98.2, 1.7, 0)	1.453	1531	1474
12	(47.5, 52.1, 0.31)	1.999	1411	1210
13	(70.6, 29.3, 0)	1.460	1539	1472

Table 3: Nomenclature, composition, and density

Specimen	Composition Description	Density of disk
3Y	100wt% 3YSZ	
8Y	100wt% 8YSZ	
Al_2O_3	100wt% Al_2O_3	
R1	48.8wt% 3Y-50.8wt% 8Y-0.35wt% Al_2O_3	5.9g/cm^3
C0	50.0wt% 3Y-50.0wt% 8Y-0wt% Al_2O_3	
C035	49.8wt% 3Y-49.8wt% 8Y-0.35wt% Al_2O_3	
C05	49.7wt% 3Y-49.7wt% 8Y-0.50wt% Al_2O_3	
C1	49.5wt% 3Y-49.5wt% 8Y-1.0wt% Al_2O_3	
C10	45.0wt% 3Y-45.0wt% 8Y-10.0wt% Al_2O_3	5.1g/cm^3
C20	40.0wt% 3Y-40.0wt% 8Y-20.0wt% Al_2O_3	4.3g/cm^3
C30	35.0wt% 3Y-35.0wt% 8Y-30.0wt% Al_2O_3	3.7g/cm^3

Table 3 shows the proportions of the mixtures, where R1 is the recommended value that was obtained through the Gaussian process regression model.

Measured a total of 3 grams of 3YSZ-8YSZ oxide from TOSOH, and pure Al_2O_3 powder from Merck, and using a ϕ 25 mm mold, performed uniaxial pressing at 8 MPa for one minute. The pressed samples were carefully transferred to an electric furnace and sintered at 1410 °C for 5 hours. The weight (m), thickness (h), and radius (r) of the samples were measured five times, and the average values were used to calculate the density. The obtained disks were polished with emery paper: #400, #800, #1000 and #1200, for one hour on each side. Finally, performed mirror polishing with a buffing wheel. Next, applied platinum paste to the samples and ensured there was no contact with the paste. As the Pt paste was manually applied, preventing perfectly parallel surfaces, ten measurement points were taken, and the average distance (L) was adopted. Heat treatment was carried out in an electric furnace at 1200 °C for 2 hours. The DC 4-terminal method was used to evaluate electrical conductivity, as shown in Fig. 4. The electrical conductivity

measurement was carried out at 900, 800, 700 and 600 °C in static air. The range of the voltage was from 1.0 to 2.5V in steps of 0.1 V. The electrical conductivity (σ) was calculated by recording the current and the voltage. Since YSZ is an oxide ionic conductor, an Arrhenius plot was used to explain the relationship between temperature and conductivity. Ea (activation energy) and A (pre-exponential function) were determined from the slope of the Arrhenius plot.

(a) Theory (b) Practical

Fig. 4. DC four-terminal method

$$\rho = m/Sh = \pi r^2 h \quad (1)$$

$$E = RI \quad (2)$$

$$R = \sigma \frac{L}{S} \quad (3)$$

$$\sigma = \frac{L}{SR} = \frac{LI}{SE} \quad (4)$$

$$\sigma T = A\exp\left(-\frac{E_a}{kT}\right) \quad (5)$$

$$\log \sigma T = \left(-\frac{1000E_a}{k}\log e\right)\frac{1}{1000T} + \log A \quad (6)$$

A Vickers hardness tester manufactured by AKASHI was used for the Vickers hardness test, employing a square pyramidal diamond indenter with an apex angle of 136°. The test conditions were 10 kgf for 15 seconds. A diamond-shaped indentation was observed. HV10 was calculated 5 times using equation (6) from the diagonals(d) of the indentation length.

$$HV = \frac{2F\sin\left(\frac{136^\circ}{2}\right)}{d^2} = 1.853\frac{F}{d^2} \quad (7)$$

The crystal structure of the powder and the disk was identified by performing X-ray diffraction (XRD; MXP3, Macscience, Ltd.) analyses using CuKα radiation. The diffraction condition is shown in Table 4. The FOX-Monte Carlo method was applied to analyze the crystal structures of undefined unit cells, such as the YSZ phase doped with alumina.

$$2D\sin\theta = n\lambda \quad (8)$$

Table 4: XRD Diffraction condition.

Method of measurement	XRD
Vacuum tube	Cu
Characteristic X-ray	Cu Kα
Voltage	40 kV
Current	40 mA
Diffraction angle	2θ
Scanning speed	0,02 °/s
Scanning range	10-90°

Surface morphology of the disks and element distribution maps measured by Scanning Electron Microscope (SEM) JEOL Ltd. JCM-6000. Metal (Au, Pt) coating was applied to the surface of the disks.

Table 5: Measurement Conditions for SEM (Secondary Electrons).

Accelerating Voltage	15.0 kV
Beam Current	7.475 nA
PHA Mode	T3
Energy Range	0 - 20 keV
Working Distance	10 mm

4. Results and Discussion

4.1 Results of XRD test

Figure 5 shows XRD patterns for 3YSZ and 8YSZ powders, the main peaks from 3YSZ and 8YSZ had appeared at the same positions. The pattern of 3YSZ was broad compared with the 8YSZ pattern, which had poor crystallinity in the 3YSZ powder. Consider that the monoclinic phase has poor crystallization. Then used FOX to analyze both materials, finding that 8YSZ exhibits a cubic structure as shown in Fig. 6(a) that was similar to the results observed with ICDD (C-YSZ # 00-030-1468), while 3YSZ exhibits a monoclinic structure as shown in Fig. 6(b) that was similar to the results observed with ICDD (m-ZrO_2 # 00-083-9444). As shown in Fig. 6(b), after excluding the two additional peaks of 3YSZ, further analysis of 3YSZ revealed that 3YSZ exhibits a tetragonal structure as shown in Fig. 6(c) that was similar to the results observed with ICDD (T-YSZ # 00-080-2187). Therefore, it can be concluded that the two peaks in Fig. 5(b) correspond to the monoclinic phase and tetragonal phase. It was consistent with the other XRD analysis study. [7]

The lattice constants for the monoclinic of 3YSZ were a = 3.221 Å, b = 5.172 Å, c = 3.614 Å, and for 8YSZ, the lattice constants for cubic were a = 5.140 Å. Additionally, the lattice constants for the tetragonal of 3YSZ were a = 5.165 Å, c = 3.603 Å. In another study, the lattice constants of the 3YSZ of a = 5.172 Å, c = 3.605 Å. It was consistent with our experimental results. [8] The crystal structure of R1 was indexed as a cubic with a lattice constant of a = 5.132 Å. This value is smaller than that of 8YSZ, based on the XRD results, it was suggested that most of the 3YSZ is dissolved into the structure of 8YSZ in the cubic of R1. In the fluorite-type structure, both Zr^{4+} and Y^{3+} were coordinated with 8 oxide-ion. The Shannon ionic radius of Zr with coordination number 8 is 0.840 Å, and that of Y with coordination number 8 is 1.019 Å. The addition of a large amount of 3YSZ to R1, which has a lower Y content than 8YSZ, results in a smaller lattice constant for R1 compared to 8YSZ powder. This is because the atomic radius of Zr is smaller than that of Y, even though both structures were cubic in nature. This is also the reason for the peak shift observed when comparing 3YSZ and 8YSZ. With more Y replacing Zr, the lattice expands, according to Bragg's Law, D increases, and θ decreases, resulting in a leftward shift of the peak.

Figure 7(a) shows XRD patterns of Adding different components of Al_2O_3 to a mixture of 8YSZ and 3YSZ. The powdered samples show three peaks at 25, 28 and 32°. In contrast, the peaks of the monoclinic phase at 25 and 28° disappeared at the disks. The disappearance of monoclinic phase peaks was still present in C0. This suggests that the disappearance of the monoclinic phase peaks at 25° and 28° was likely due to heat treatment and was a characteristic of the 3YSZ and 8YSZ mixture, independent of the presence of Al_2O_3. As shown in Fig. 7(b), the XRD patterns of the disk of R1, C1, C05, and C0 were indexed as cubic zirconia phases. This indicates that the crystalline structure has transformed from the initial monoclinic and tetragonal phases to the cubic phase. Subsequent analysis of the XRD of samples with small amounts of Al_2O_3 added (C0, C05, C1, R1) revealed that did not find peaks corresponding to

Al_2O_3 and peak shift. By increasing the alumina content (C10, C20 and C30), observed in Fig. 7(b) that the characteristic peaks of Al_2O_3 gradually became more distinct, while the characteristic peaks of YSZ weakened. This observation aligns with the results of other studies. [9] However, no peak shift was detected when comparing these samples, indicating that solid solution characteristics cannot be observed through XRD analysis. But in another study, the phenomenon of Al_2O_3 and Zr_2O_3 solid solution was discovered by comparing lattice constants in 8YSZ and 8YSZ-Al_2O_3, with a limit of only 0.3wt%. [10] Although our study added 3YSZ compared to it, we believe it was still of reference value. The absence of characteristic peaks at low alumina content suggests that the alumina concentration was below the detection limit of XRD resolution. Moreover, the very low solubility limit of alumina in YSZ likely accounts for the lack of observable peak shifts, even with increased alumina content. The peak positions were shown in Fig. 7(b), where the peaks corresponding to Al_2O_3 were indicated by triangles and peaks of YSZ were represented by circles.

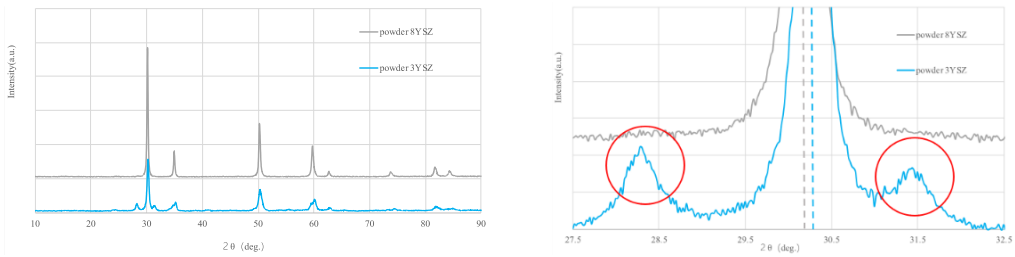

(a) Comprehensive (b) Local

Fig. 5. XRD patterns from 8YSZ and 3YSZ

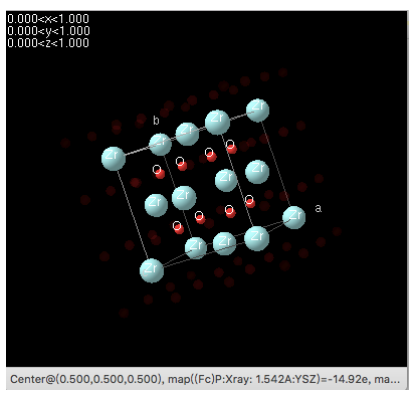

(a) Cubic 8YSZ

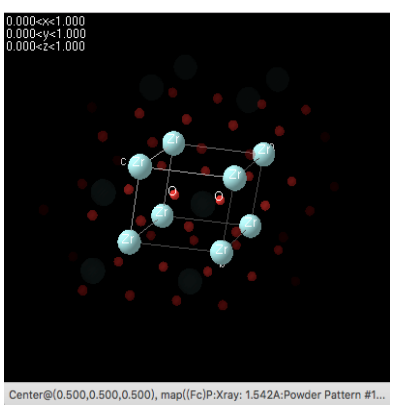

(b) Monoclinic 3YSZ

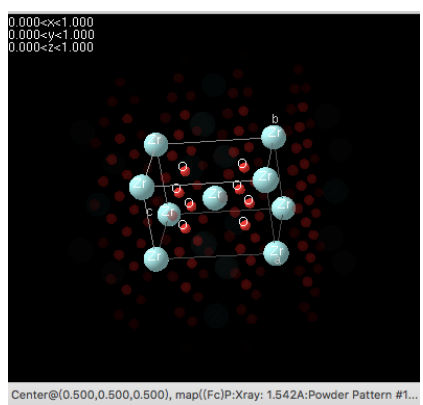

(c) Tetragonal 3YSZ

Fig. 6. Crystal structure of 8YSZ and 3YSZ

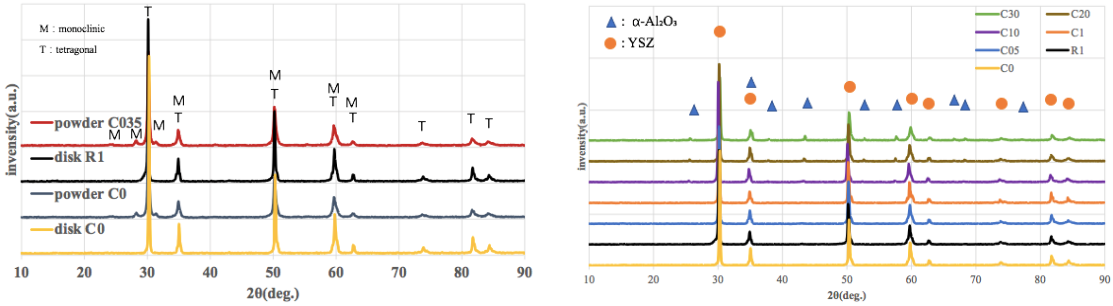

(a) C035, R1 and C0 (disks and powder) (b) Disks of C30, C20, C10, C1, C05, R1, C0

Fig. 7. XRD patterns of Adding different components of Al_2O_3 to a mixture of 8YSZ and 3YSZ

4.2 Morphologies on the disk surfaces of 3YSZ-8YSZ-Al_2O_3 systems and the element distribution maps.

Figure 8 shows SEM and EDS data on the surface of the 3YSZ-8YSZ disk with C30. Secondary particles of about 10 microns and primary particles of several microns were observed. X-rays from Zr, Y, Al, C and O were observed by EDS from the observation field. There were dark and light areas in the SEM image.

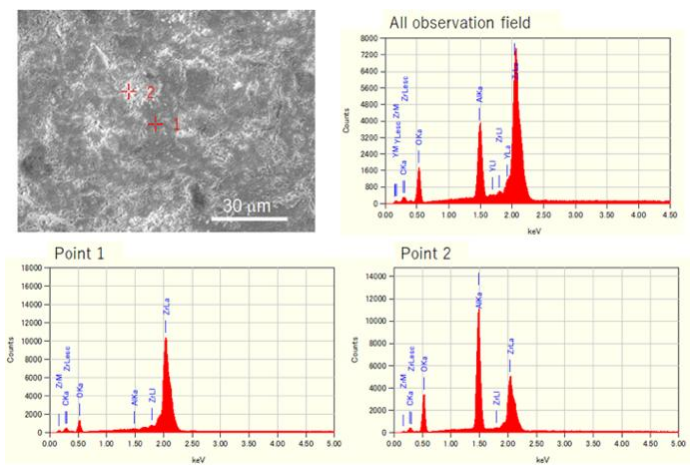

Fig. 8. SEM and EDS data on the surface of the 3YSZ-8YSZ disk with C30.

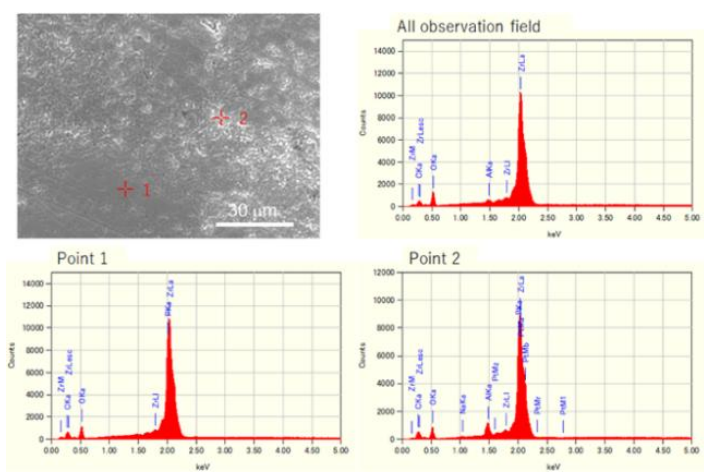

Fig. 9. SEM and EDS data on the surface of the 3YSZ-8YSZ disk with R1.

At a typical dark area, point 1, Zr was strongly observed. At the light area, point 2, Zr and Al were observed. Figure 9 shows SEM and EDS data on the surface of the 3YSZ-8YSZ disk with R1. Primary particles of several microns were observed. EDS revealed the presence of Zr, Al, C and O from the observation field. The dark and light areas were also observed in the SEM image. At the typical dark area, point 1, Zr was strongly observed and at point 2 of the light area, Zr and Al were observed. To make the sample easier to observe, platinum was sputtered onto the sample surface. However, a brightly charged observation area appeared. It was thought that this area was observed brighter because it was less conductive than other areas due to the presence of Al_2O_3.

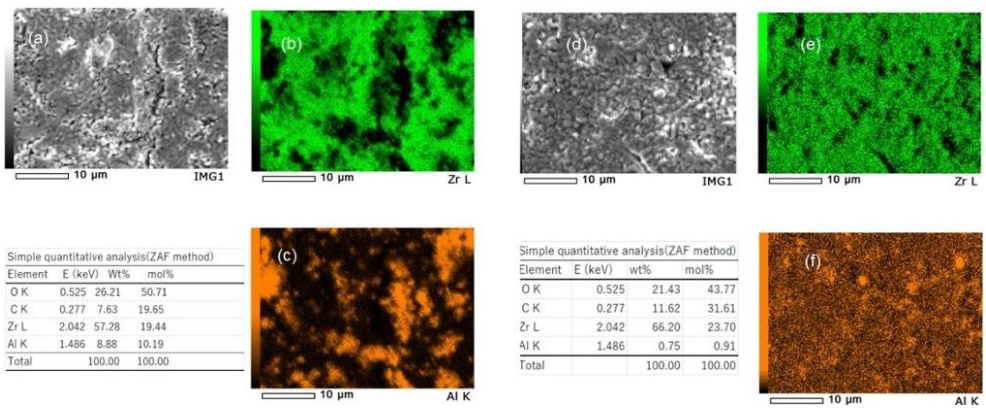

Fig. 10. SEM images and EDS maps. (a) SEM image of 3YSZ-8YSZ disk with C30, (b) Zr distribution map, (b) Al distribution map, (d) SEM image of 3YSZ-8YSZ disk with R1, (e) Zr, and (f) Al distribution map.

Figure 10 shows SEM images and EDS maps for C30 and R1. On the disk of C30, as shown in Fig. 10b, Zr was distributed on the surface of the dark areas in Fig. 10(a). Near the cracks, Al was observed in contrast to Zr shown in Fig. 10(c). It has been reported that this distribution and aggregation of trivalent Al can occur in the early stage of the sintering process. [4] The amount of ZrO_2 and Al_2O_3 in C30, estimated by the ZAF method, were 82.1 and 17.9wt% respectively. The amount of Al_2O_3 was less than the amount weighed because Al_2O_3 has entered the cracks, and a small amount of trivalent Al has diffused into tetravalent Zr. These decreases in the lattice parameters (increase of the peak angles) are according to Vegard's Law. On the disk for R1, Zr and Al were almost uniformly present (Fig. 10(e and f)). On the disk surface of R1, it was confirmed that the distribution was more uniform throughout than on the disk surface of C30. Agglomeration of Al element was observed in some cracks especially (Fig. 10(f)). The amount of ZrO_2 and Al_2O_3 were estimated at 98.9 and 1.1wt% respectively. The amount of Al_2O_3 is nearly three times larger than the amount of preparation (R1). This might be due to the resolution of EDS.

4.3 Effect of the Al_2O_3 addition on electrical conductivity

In this experiment, we measured the conductivity of disk R1 and compared it with the conductivity of disk C0, which did not contain additive Al_2O_3. As shown in Fig. 11 the electrical conductivity of all samples decreases with a decrease in temperature and observed a similar rate of decline. The R1 exhibited significantly higher electrical conductivity and the logσT was approaching 5.4 at 900°C. In other temperatures, it was also higher than C0. In contrast, the sample without added aluminum oxide has a much lower electrical conductivity than the R1. It was precisely through machine learning that this optimal ratio could be accurately determined.

To Compare another study, at a high temperature of 1000°C, the highest conductivity of the 8YSZ and Al_2O_3 mixture (ranging from 0wt% to 30wt%) reached logσT of 2.2, whereas the R1 was observed logσT of 5.4. After removing the log scale, the electrical conductivity of R1 was 10^3 times higher, and its operating temperature was only 900°C. [6] In another experiment, the best performance (pure 8YSZ) across the entire temperature range occurred at 900°C, reaching an electrical conductivity of around logσT of 2.1. Similarly, when the log scale was removed, the electrical conductivity of R1 was about 10^3 times higher. As the temperature decreased, the decline in electrical conductivity observed in this study was very close to the values reported in our results. [12] The Pre-exponential Factor (A) of C0 was $10^{8.38}$ (S K/m) and Activation Energy (Ea) of C0 was 0.881 eV. The Pre-exponential Factor (A) of R1 was $10^{10.09}$ (S K/m) and Activation Energy (Ea) of R1 was 1.12 eV. In other studies, the activation energy of 8YSZ is 0.774 eV, while that of 3YSZ is 0.901 eV.[11] This indicates that although the rate of decrease in electrical

conductivity for R1 was slightly higher than that of C0, 3YSZ, and 8YSZ as the temperature decreased, the difference was insignificant. Furthermore, due to its significantly high Pre-exponential Factor, R1 demonstrates high conductivity at elevated temperatures and has the potential to maintain good conductivity at lower temperatures.

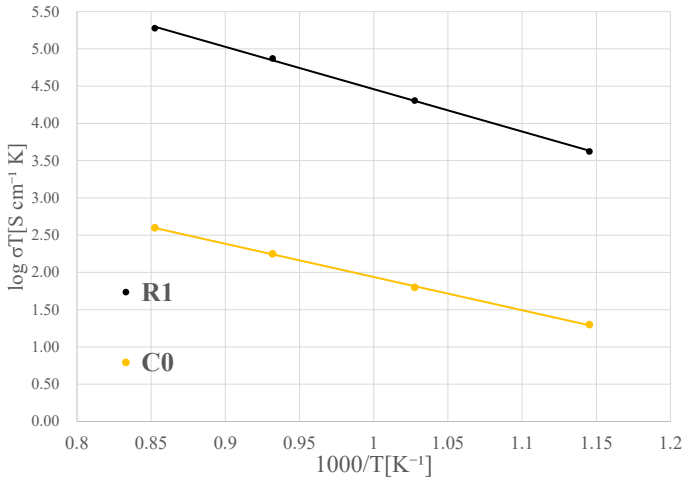

Fig. 11 Electrical conductivity with Varying Aluminum Oxide Content.

4.4 Effect of Al_2O_3 addition on Vickers hardness test

In Figure 12, Vickers hardness shows a decreasing trend with the addition of Al_2O_3. The R1 had the highest hardness among all samples with added Al_2O_3, showing no significant decrease compared to the C0, and maintained above the common solid electrolyte materials 3YSZ that was 1295(HV10) and 8YSZ that was 1204(HV10). [12]

In Figure 12, a decrease in hardness was observed with increasing Al_2O_3 content. YSZ underwent grain growth under high-temperature conditions [13], but when Al_2O_3 was added within the solubility limit, the grain boundaries were pinned by the solid solution phase, which controlled grain migration and growth. Considered that the solid solution of Al_2O_3 can range from 0 to 0.3wt%, where Al_2O_3 can be in solid solution, the Vickers hardness remains almost constant. However, at 0.35wt%, the hardness decreased slightly. As shown in Figure 10(f), Al_2O_3 beyond the solid solution limit was agglomerated at the YSZ interface. This agglomeration may have caused the decrease in Vickers hardness. This phenomenon became more pronounced with increasing alumina content and the Vickers hardness is considered to have decreased. The Vickers hardness is usually closely correlated with the yield strength and tensile strength of the material. The test measures the resistance of material to deformation by pressing a diamond indenter into its surface, reflecting its ability to resist plastic deformation. Higher hardness typically indicates higher yield strength and tensile strength. Therefore, we believed that the mechanical strength correspondingly improved as Vickers hardness increased.

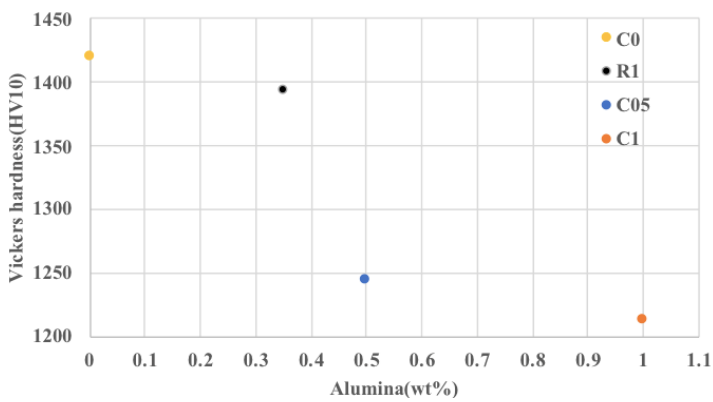

Fig. 12 Vickers hardness

5. Conclusion

In this experiment, the crystal structure of R1 was cubic with a lattice constant of a=5,132 Å. Peaks corresponding to monoclinic and tetragonal phases observed in the powder disappear upon heating, suggesting that the cubic structure becomes the main phase. Based on the SEM and EDS results, it was observed that Al_2O_3 was uniformly dispersed in R1. On the surface of the C30 sample, cracks and Al_2O_3 aggregation were observed. The conductivity of R1 was higher than that of the other samples across the entire temperature range. The Vickers hardness decreases with an increase in the content of Al_2O_3. Although the Vickers hardness of R1 decreased compared to C0, it remains higher than that of C05 and C1, exceeding the expected value. In summary, we used machine learning to obtain ratio data recommended by the computer. The R1 produced using this ratio has excellent electrical conductivity while maintaining Vickers hardness.

Acknowledgment

Appreciation is due to Professor Takuya Hashimoto from the Department of Physics, College of Humanities and Sciences, Nihon University, for assistance in the fabrication of electrolyte disks, which significantly contributed to the progress of the study. We also thank Dr. Kenji Honma of Fujitsu Limited for providing the machine-learning data that greatly contributed to the progress of this research.

Nomenclature

L	Distance from platinum paste to platinum paste, m
S	Surface area of the electrolyte disk, m^2
σ	electrical conductivity, S/m
I	currently, A
E	voltage, V
T	Kelvin, K
R	electrical resistance, Ω
ρ	density, kg/m^3
h	thickness of disks, m
m	weight of disk, kg
r	radius of disk, m
A	Pre-exponential factor, S K/m
Ea	Activation Energy, eV
k	Boltzmann constant
HV	Vickers hardness, HV10
F	load, kg/f
d	average diagonal length, m
D	Lattice plane spacing, Å
θ	Incident angle of the X-ray
λ	Wavelength of the incident X-ray
n	Any integer

References

[1] Tojo T, Kawaji H, Atake T. Low temperature heat capacity and lattice defects of stabilized zirconia. Journal of the Ceramic Society of Japan (J-STAGE). 2000;27(4):186–194.

[2] Ueno T, Rhone TD, Hou Z, Mizoguchi T, Tsuda K. COMBO: an efficient Bayesian optimization library for materials science. Materials Discovery. 2016;4:18–21.

[3] Homma K, Liu Y, Sumita M, Tamura R, Fushimi N, Iwata J, Tsuda K, Kaneta C. Optimization of a heterogeneous ternary Li_3PO_4–Li_3BO_3–Li_2SO_4 mixture for Li-ion conductivity by machine learning. Journal of Physical Chemistry C. 2020;124:12865–12870.

[4] Yoshinaga M, Katoh H, Fujimoto Y. Vickers hardness and electrical conductivity of 3YSZ/8YSZ. Composite Bulletin of the School of Engineering, Tokai University. 2022;62(1):9–13.

[5] Danilenko V, Lakusta V, Loladze T, Volkova E, Popov V, Glazunova E, Konstantinova T. Effect of Al_2O_3 added by mechanical mixing and co-doping on the densification mechanisms of zirconia nanoparticles at the initial stage of sintering. Results in Physics. 2020;9:103495.
[6] Feighery AJ, Irvine JTS. Effect of Al_2O_3 additions upon electrical properties of 8 mol% yttria-stabilized zirconia. Solid State Ionics. 1999;121:209–216.
[7] Herrera AM, de Oliveira Jr AAM, de Oliveira APN, Hotza D. Processing and characterization of yttria-stabilized zirconia foams for high-temperature applications. Journal of Ceramics. 2013;2013:785210.
[8] Chislov MV, Borik MA, Kulebyakin AV, Lomonova EE, Milovich FM, Myzina VA, Parkhomenko YuN, Ryabochkina PA, Sidorova EV, Tabachkova NYu. Comparison of mechanical properties of zirconia crystals partially stabilized with yttria and gadolinia. Journal of Physics: Conference Series. 2019;1347:012059.
[9] Noroozpour M, Akbari A. YSZ–Al_2O_3 thermal barrier nanocomposite coatings: electrophoretic deposition and characterization. Journal of the American Ceramic Society – Journal of Applied Ceramic Technology. 2023;21(2):888–899.
[10] Tekeli S. The solid solubility limit of Al_2O_3 and its effect on densification and microstructural evolution in cubic zirconia used as an electrolyte for solid oxide fuel cells. Materials & Design. 2007;28(2):713–716.
[11] Al-Attara AF, Farid SBH, Hashim FA. Characterizations of synthetic 8 mol% yttria-stabilized zirconia with comparison to 3 mol% yttria-stabilized zirconia for high-temperature solid oxide fuel cells. Engineering and Technology Journal. 2020;38(Part A, No. 4):491–500.
[12] Ghatee MH, Shariat MH, Irvine JTS. Investigation of electrical and mechanical properties of 3Y-TZP/cubic zirconia solid electrolytes with composite structure prepared by near net shape forming. Solid State Ionics. 2009;180:904–909.
[13] Mohd Affandi NS, Osman N. Short review on global trends in solid oxide fuel cell scenario and future perspective. Materials Today: Proceedings. 2022;66:3981–3984.